

# The Adsorption of H<sub>2</sub>O on TiO<sub>2</sub> and SnO<sub>2</sub> (110) Studied by First-Principles Calculations

J. Goniakowski and M. J. Gillan

*Physics Department, Keele University, Staffordshire ST5 5BG, U.K.*

**Abstract:** First-principles calculations based on density functional theory and the pseudopotential method have been used to investigate the energetics of H<sub>2</sub>O adsorption on the (110) surface of TiO<sub>2</sub> and SnO<sub>2</sub>. Full relaxation of all atomic positions is performed on slab systems with periodic boundary conditions, and the cases of full and half coverage are studied. Both molecular and dissociative (H<sub>2</sub>O → OH<sup>-</sup> + H<sup>+</sup>) adsorption are treated, and allowance is made for relaxation of the adsorbed species to unsymmetrical configurations. It is found that for both TiO<sub>2</sub> and SnO<sub>2</sub> an unsymmetrical dissociated configuration is the most stable. The symmetrical molecularly adsorbed configuration is unstable with respect to lowering of symmetry, and is separated from the fully dissociated configuration by at most a very small energy barrier. The calculated dissociative adsorption energies for TiO<sub>2</sub> and SnO<sub>2</sub> are in reasonable agreement with the results of thermal desorption experiments. Calculated total and local electronic densities of states for dissociatively and molecularly adsorbed configurations are presented and their relation with experimental UPS spectra is discussed.

## 1 Introduction

Most oxide surfaces react readily with water and become partially covered with molecular H<sub>2</sub>O or hydroxyl groups on exposure to air under ambient conditions. This adsorption of water has important consequences for surface processes such as catalysis and gas sensing. It is widely accepted that molecular water will generally bind to most oxide surfaces through the attraction of its electric dipole to the ionic charges. However, the mechanisms by which dissociative adsorption occurs are still very poorly understood. It has sometimes been suggested that surface defects such as vacancies or steps are essential to water dissociation, and there is no doubt that there are some oxide surfaces for which this is true. For example, recent calculations using both semi-empirical [1] and first-principles [2,3] techniques have shown that water dissociation is not energetically favorable on the perfect MgO (100) surface, but that it is favorable at steps and corners. However, it is unlikely that defects are essential for dissociative adsorption in general, since oxide surfaces vary enormously in their geometry and electronic structure.

The aim of this paper is to present first principles calculations on the energetics of H<sub>2</sub>O adsorption on the SnO<sub>2</sub> and TiO<sub>2</sub> (100) surfaces. Both materials have the rutile crystal structure, and the (110) surface is the most stable when the materials are stoichiometric. The stoichiometric (110) surface is far from flat, so we are dealing with a situation which is geometrically very different from the MgO (100) surface. Although they have the same geometry, SnO<sub>2</sub> and TiO<sub>2</sub> are electronically different, since Ti is a transition element and Sn is a group IV element. Our hope is therefore that by comparing with previous work on the interaction of H<sub>2</sub>O with MgO (100) we can learn about the influence both of geometry and of electronic structure. Our choice of SnO<sub>2</sub> and TiO<sub>2</sub> is also motivated by their technological importance. SnO<sub>2</sub> is widely used in gas-sensing devices, and adsorbed water is known to have an important effect on the adsorption of other molecules [4]. The interaction of TiO<sub>2</sub> with water is important in photocatalytic applications [5].

A considerable experimental effort has gone into the study of H<sub>2</sub>O adsorption on TiO<sub>2</sub> (110), though a clear picture has yet to emerge. Hydroxyl groups on the surface have been detected at 300 K in ultraviolet photoelectron spectroscopy (UPS) experiments by Henrich *et al.* [6], and their presence was later confirmed in synchrotron radiation studies by Madey's group [7,8]. The amount of dissociated water was less than a monolayer, and was weakly dependent on the oxygen vacancy concentration before adsorption. The minor influence of point defects and steps on the reactivity with water has also been reported by Muryn *et al.* [9]. Experiments using a combination of thermal desorption spectroscopy (TDS), x-ray photoelectron spectroscopy (XPS) and work-function measurements have recently been reported [10]. A three-peak desorption spectrum was found, with features at 170 and ~275 K and a high-temperature tail up to ~375 K. The two low-temperature features appear to be due to molecular water and the high-temperature tail to the reaction of surface OH groups to form H<sub>2</sub>O. A widely accepted model is that of Kurtz *et al.* [7], who proposed that adsorption on nearly perfect TiO<sub>2</sub> (110) occurs by molecular adsorption of H<sub>2</sub>O at 5-fold coordinated cation sites, followed by dissociation to give OH<sup>-</sup> attached by its oxygen end to the cation, and H<sup>+</sup> bonded to lattice oxygen to form a second type of hydroxyl group. The presence of at least two types of adsorbed OH<sup>-</sup> has been indicated by infrared spectroscopy [11,12].

The experimental situation for SnO<sub>2</sub> is rather similar, although the experimental evidence is less extensive. Recent experiments by Gercher and Cox [13] using a combination of TDS and UPS show the presence of dissociatively adsorbed water on SnO<sub>2</sub> (110). On the perfect stoichiometric surface, three distinct TDS peaks are seen at  $T = 200, 300$  and 435 K. The 200 K peak is attributed entirely and the 300 K peak mainly to molecular H<sub>2</sub>O. The feature at 435 K is assigned to disproportionation of surface OH<sup>-</sup> to form H<sub>2</sub>O. As in the case of TiO<sub>2</sub>, surface defects do not appear to play a major role.

Few theoretical investigations of H<sub>2</sub>O adsorption on rutile surfaces have been reported. Jaycock and Waldsax [14] performed calculations for the TiO<sub>2</sub> (110) and (100) surfaces using an empirical interaction model, which predicted adsorption energies much greater than the experimental values. The dissociative adsorption of single molecules on clusters embedded in a point-charge lattice has been studied using the  $X\alpha$  approach for TiO<sub>2</sub> (110) by Tsukada *et al.* [15]. The dissociative adsorption of single water molecules on TiO<sub>2</sub> as well as the case of full

hydroxylation have been studied using a semi-empirical technique by Goniakowski *et al.* [16] and Goniakowski and Noguera [1]. Both molecular and dissociative adsorption of water on  $\text{TiO}_2$  have been treated using a periodic Hartree-Fock approach by Fahmi and Minot [17], who find a strong preference of water to dissociate. The above studies considered only very symmetrical configurations of adsorbed species, and all found that both molecular and dissociative adsorption are energetically favorable. The only attempt to study relaxation of surface species to unsymmetrical configurations has been the very recent semi-empirical study by Bredow and Jug on the adsorption of  $\text{H}_2\text{O}$  on rutile and anatase  $\text{TiO}_2$  surfaces [18]. To our knowledge no theoretical attempts to model water adsorption on  $\text{SnO}_2$  surfaces have been reported.

The present work is based on density functional theory (DFT) in the pseudopotential approximation. This approach has been widely used for oxides, including  $\text{MgO}$  [19],  $\text{Li}_2\text{O}$  [20],  $\text{Al}_2\text{O}_3$  [21],  $\text{TiO}_2$  [22,23] and  $\text{SnO}_2$  [24], and is known to give accurate results for the energetics of perfect crystals, lattice defects, surfaces and molecular adsorption. We have recently reported a detailed study of the stoichiometric and reduced  $\text{SnO}_2$  (110) surface using this approach [25]. However, since the energetics of dissociation is not generally described very accurately within the standard local density approximation (LDA), we include gradient corrections in the present work, using the Becke-Perdew scheme [26,27]. We present here results on the energetics and relaxed geometry of both molecularly and dissociatively adsorbed water on  $\text{SnO}_2$  and  $\text{TiO}_2$  (110), and we study both symmetrical and unsymmetrical modes of adsorption. In addition, we report total and local electronic densities of states, through which we attempt to make contact with recent spectroscopic measurements.

## 2 Techniques

### 2.1 General background

The general principles of DFT and the pseudopotential method have been described in the literature [28–32]. Within the pseudopotential approximation only valence electrons are represented explicitly in the calculations, the valence-core interaction being represented by non-local pseudopotentials which are generated by first principles calculations on isolated atoms. The calculations are performed using periodically repeating geometry, the occupied orbitals being expanded in a plane wave basis. This expansion includes all plane waves whose kinetic energy  $E_k = \hbar^2 k^2 / 2m$  ( $k$  the wavevector,  $m$  the electron mass) is less than the cut-off energy  $E_{\text{cut}}$ , chosen so as to ensure convergence with respect to the basis set.

In the present work the self-consistent ground state of the system was determined using a band-by-band conjugate gradient technique to minimize the total energy of the system with respect to the plane-wave coefficients. Equilibrium positions of ions were determined by a steepest descent method. The calculations were performed using the CETEP code [33] (the parallel version of the serial code CASTEP [32]), running on the 64-node Intel iPCS/860 machine at Daresbury Laboratory.

## 2.2 Generalized Gradient Corrections

Standard DFT calculations make use of the LDA, which treats the electron density as locally uniform. Although this is highly successful for many purposes, it does not give accurate results for energy differences involving changes of bonding, which are of interest here. In the last few years, methods have been developed for improving the LDA through ‘generalized gradient’ approximations (GGA). It has been shown that these corrections lead to improvement in the calculation of total energies of atoms and molecules [27,34–39], cohesive energies [40–42], and the energetics of molecular adsorption and dissociation on metal surfaces [43–46]. We have recently reported a comparison of the influence of two popular GGA schemes – those due to Perdew and Wang [27,36] and Becke and Perdew [26,27]) – on the bulk and surface properties of TiO<sub>2</sub> and SnO<sub>2</sub> [47]. We found that the Becke-Perdew method gives better equilibrium lattice parameters, while giving essentially the same surface properties as Perdew-Wang, and we employ Becke-Perdew in the present work. We use the technique of White and Bird [48] for incorporating GGA within the DFT-pseudopotential calculation. In some places, we shall also report LDA results for comparison; these were obtained using the Ceperley-Alder (CA) exchange-correlation function [49].

## 2.3 Generation of pseudopotentials

First-principles, norm-conserving pseudopotentials in Kleinman-Bylander representation [50] were generated using the optimization scheme of Lin *et al.* [51] in order to reduce the required value of the plane-wave cut-off  $E_{\text{cut}}$ . The pseudopotentials used in GGA calculations were constructed in a consistent way by including GGA in the generation scheme. The Sn pseudopotential was generated using the  $5s^25p^2$  configuration for  $s$ - and  $p$ -wave components, and the  $5s^15p^{0.5}5d^{0.5}$  configuration for the  $d$ -wave. The core radii were equal to 2.1, 2.1 and 2.5 a.u. for the  $s$ ,  $p$  and  $d$  components respectively. The Ti pseudopotential was generated using the  $4s^{1.85}3d^2$  configuration for the  $s$  and  $d$  waves and the  $4s^14p^{0.5}3d^{0.5}$  configuration for the  $p$  wave, with core radii of 2.2, 1.5 and 2.4 a.u. for  $s$ ,  $p$  and  $d$  waves respectively. The oxygen pseudopotential used in our LDA calculations was generated using the  $2s^22p^4$  configuration for the  $s$  and  $p$  waves and the  $2s^22p^{2.5}3d^{0.5}$  configuration for the  $d$  wave, with a single core radius of 1.65 a.u. For the gradient-corrected oxygen pseudopotential, we have used the single configuration  $2s^22p^{3.5}3d^{0.45}$  and the same core radius. The use of a core radius of 1.65 a.u. means that there is an appreciable overlap of the oxygen and metal core spheres in the SnO<sub>2</sub> and TiO<sub>2</sub> crystals, and in principle this could cause inaccuracies. However, direct comparisons of the present results with our earlier work on SnO<sub>2</sub> [25], which employed an oxygen pseudopotential with the smaller core radius of 1.25 a.u., show that any errors due to core overlap are very small.

The calculations have been done using a plane wave cut-off of 600 eV for SnO<sub>2</sub> and 1000 eV for TiO<sub>2</sub>. Our tests show that with these cut-offs the energy per unit cell is converged to within 0.2 eV.

Fig. 1. The unit cell of the rutile crystal structure. Cations are represented by small black circles and oxygen atoms by large white circles.

Fig. 2. Atomic structure of the clean (110) surface. 6- and 5-fold coordinated cations are represented by small black circles and small black circles with white centers respectively. In plane oxygen atoms are represented by large white circles and bridging oxygens by large gray circles.

## 2.4 Densities of States

Electronic densities of states (DOS) associated with the ground state were calculated using the tetrahedron method [52,53], with  $k$ -point sampling corresponding to 750 tetrahedra in the whole Brillouin zone. In addition, local densities of states (LDOS) were calculated by taking contributions only from chosen regions of real space – in practice we have used spheres (radius 1.5 Å) centered on chosen surface oxygen atoms. For presentation purposes, we have broadened the calculated DOS and LDOS by Gaussians of width 0.5 eV. In the ground state calculations the Brillouin zone sampling is performed using the lowest order Monkhorst-Pack set of  $k$  points [54], as in our previous work on SnO<sub>2</sub> [24,25].

## 3 Tests on SnO<sub>2</sub>, TiO<sub>2</sub> and H<sub>2</sub>O

### 3.1 Perfect crystals and (110) surfaces

A more detailed discussion of the influence of gradient corrections on the calculated parameters of the SnO<sub>2</sub> and TiO<sub>2</sub> perfect crystals and (110) surfaces is given in a separate paper [47]. Here we present the system used in the calculations and recall the principal results obtained using the Becke-Perdew GGA scheme.

The six-atom rutile unit cell of SnO<sub>2</sub> and TiO<sub>2</sub> is shown in Fig. 1. The equilibrium structure has been determined by relaxation with respect to the lattice parameters  $a$  and  $c$  and the internal parameter  $u$ . The equilibrium values of these parameters calculated using the Becke-Perdew form of GGA are given in Table 1. The agreement of  $a$  and  $c$  with experiment is very satisfactory for SnO<sub>2</sub> and acceptable for TiO<sub>2</sub>; the values of  $u$  are excellent in all cases.

Our calculations on the stoichiometric (110) surface of the materials have been done with the usual repeating slab geometry. The rutile structure can be regarded as consisting of (110) planes of atoms containing both metal (M) and oxygen (O) atoms, separated by planes containing oxygen alone, so that the sequence of planes is O - M<sub>2</sub>O<sub>2</sub> - O - O - M<sub>2</sub>O<sub>2</sub> - O etc. The entire crystal can then be built up of the symmetrical 3-plane O - M<sub>2</sub>O<sub>2</sub> - O units. The slabs we use contain three of these units, and our repeating cell contains 18 atoms (6 M and 12 O). The perfect (110) surface consists of rows of bridging oxygens lying above a metal-oxygen layer (see Fig. 2). The vacuum separating the slabs has been taken wide enough to ensure that interactions

Table 1

Comparison of theoretical and experimental [55] values of lattice parameters  $a$  and  $c$  and the internal coordinate  $u$  of  $\text{SnO}_2$  and  $\text{TiO}_2$ . The theoretical values are calculated using the Becke-Perdew form of GGA.

	$\text{SnO}_2$		$\text{TiO}_2$	
	calc.	expt.	calc.	expt.
$a$ (Å)	4.809	4.737	4.747	4.594
$c$ (Å)	3.159	3.186	3.039	2.958
$c/a$ (Å)	0.657	0.673	0.640	0.644
$u$ (Å)	0.307	0.307	0.305	0.305

Fig. 3. Calculated valence band DOS for clean (110) surfaces of  $\text{TiO}_2$  and  $\text{SnO}_2$ . The dashed line represents the LDOS on the bridging oxygen site  $\text{O}_I$ . For the sake of presentation the local contribution has been scaled by a factor of 5.

between neighboring slabs are small even when adsorbed  $\text{H}_2\text{O}$  and  $\text{OH}^-$  are present. The width we use corresponds to two O -  $\text{M}_2\text{O}_2$  - O units, and is such that planes of bridging oxygens on the surfaces facing each other across the vacuum are separated by about 6.8 Å. This vacuum width is somewhat greater than was used in our earlier calculations on  $\text{SnO}_2$  (110) [25]. (It will be convenient in the following to specify slab thickness and vacuum width in terms of the equivalent width of O -  $\text{M}_2\text{O}_2$  - O units.)

The surface structure has been determined by relaxing the entire system to equilibrium. As in our previous work on  $\text{SnO}_2$  (110), and the work of Ramamoorthy *et al.* on  $\text{TiO}_2$  (110) [22], we find displacements of the surface atoms of order 0.1 Å, with 5-fold and 6-fold coordinated metal atoms moving respectively into and out of the surface, in-plane oxygens moving out and bridging oxygens moving very little. The modifications of the bond lengths between the surface atoms with respect to the perfect crystal for Becke-Perdew GGA calculations are given in Table 2.

We find that the relaxed surface energy of  $\text{SnO}_2$  (110) is  $1.16 \text{ Jm}^{-2}$  and  $0.84 \text{ Jm}^{-2}$  for  $\text{TiO}_2$  (110). These energies are, as already discussed in Ref. [47], substantially lower than the corresponding LDA results.

The electronic DOS and the LDOS on bridging oxygen calculated for the valence band of the slab systems using the Becke-Perdew form of GGA are shown in Fig. 3. The main features of the calculated surface DOS of  $\text{SnO}_2$  have already been discussed in our previous paper [25]. We note particularly the splitting off of a narrow band of states at the top of the O(2s) band and the appearance of a sharp peak at the top of the O(2p) valence band. Both these features are associated with bridging oxygens. The features are also present for  $\text{TiO}_2$ , although the splitting

Table 2

Calculated bond length modifications on SnO<sub>2</sub> (110) and TiO<sub>2</sub> (110) with respect to the bulk values for Becke-Perdew GGA exchange-correlation. For atom indexing see Fig. 2

	SnO <sub>2</sub>	TiO <sub>2</sub>
O <sub>I</sub> – M <sub>I</sub>	-3.8%	-5.5%
O <sub>IV</sub> – M <sub>II</sub>	-4.2%	-5.6%
O <sub>II</sub> – M <sub>II</sub>	-1.2%	-1.2%
O <sub>II</sub> – M <sub>I</sub>	2.9%	2.8%
O <sub>III</sub> – M <sub>I</sub>	4.8%	4.5%

is less marked.

### 3.2 H<sub>2</sub>O and OH<sup>-</sup> molecules

We have calculated the equilibrium geometry and electronic structure of the H<sub>2</sub>O and OH<sup>-</sup> molecules. Since our techniques require us to use periodic boundary conditions, the calculations are actually performed on periodic arrays of molecules, with the repeating cell chosen to be a cube of side  $R$ . For H<sub>2</sub>O, we find that the choice  $R = 7 \text{ \AA}$  is large enough to render the interactions between periodic images negligible. Matters are not so simple for the OH<sup>-</sup> molecule, since it carries a net charge. To make mathematical sense of calculations in which the repeating cell is charged, it is essential to introduce a uniform compensating background, whose charge density is chosen so that the net charge in the unit cell vanishes. This technique is well established, and has often been discussed in the literature. However, as discussed by Leslie and Gillan [56], the total energy still converges very slowly with increasing cell size, and the leading term in its deviation from the asymptotic value is  $-\alpha/R$ , where  $\alpha$  is the Madelung constant for the appropriate periodic array of point charges. This leading correction can therefore be subtracted exactly, and we are left with a total energy which converges reasonably quickly to the value for the molecule in free space. In our calculations on OH<sup>-</sup>, we find that the corrected total energy is converged to better than 0.1 eV for  $R = 13 \text{ \AA}$ , and the equilibrium bond length is converged well before this. Comparison of the calculated and experimental structural parameters of H<sub>2</sub>O and OH<sup>-</sup> (Table 3) confirms that the molecules are described accurately by the present methods.

Since we are concerned with dissociation of H<sub>2</sub>O in this paper, we have tested the influence of the GGA on its dissociation energy. The reaction of interest is  $\text{H}_2\text{O} \rightarrow \text{OH}^- + \text{H}^+$ . To compare our results with experimental data, we start from the experimental dissociation energy for the reaction  $\text{H}_2\text{O} \rightarrow \text{OH} + \text{H}$ , which is 5.11 eV. We add to this the ionization energy of H (13.60 eV) and we subtract the electron affinity of OH (1.83 eV), to obtain 16.88 eV. Finally, addition of the

Table 3

Comparison of theoretical and experimental values of bond lengths  $d_{O-H}$  and bond angle  $\angle H-O-H$  of  $H_2O$  and  $OH^-$ . The theoretical values are calculated using the Ceperley-Alder form of LDA (CA), and the Becke-Perdew form of GGA (BP). Experimental values are taken from Refs. [57,58]

		$d_{O-H}$ (Å)	$\angle H-O-H$
$H_2O$	CA	0.977 (2.1%)	104.8 (0.3%)
	BP	0.975 (1.9%)	103.6 (-0.9%)
	expt.	0.957	104.5
$OH^-$	CA	0.980 (1.0%)	
	BP	0.979 (0.9%)	
	expt.	0.970	

zero-point vibrational energy of  $H_2O$  (0.57 eV) and subtraction of the corresponding quantity for  $OH$  (0.23 eV) gives us the value 17.22 eV which can be compared with the calculations. The calculated values with LDA and GGA are 16.6 and 16.7 eV, so that even with gradient corrections there is a residual error of  $\sim 0.5$  eV.

In order to compare with the electronic DOS reported later, it is useful to note that the single-particle energies of the occupied molecular orbitals (MO) of  $H_2O$  can be related to experimental measurements. As usual, one must be cautious about comparing Kohn-Sham single particle energies with spectroscopic energies, but it is known empirically that for occupied states the comparison is usually justified. We therefore compare the differences of our calculated MO energies with the corresponding differences of measured ionization energies. In the usual notation, the MO states of  $H_2O$  are  $2a_1$ ,  $1b_2$ ,  $3a_1$  and  $1b_1$ . Our calculated separations of  $2a_1 - 1b_2$ ,  $1b_2 - 3a_1$  and  $3a_1 - 1b_1$  (experimental values from ref. [59] in parentheses) are 11.96 eV (13.6 eV), 3.64 eV (3.8 eV) and 2.12 eV (2.0 eV) respectively. Our calculated separations of  $2\sigma - 3\sigma$  and  $3\sigma - 1\pi$  levels in  $OH^-$  are respectively 12.2 eV and 3.5 eV.

#### 4 Surface adsorption of $H_2O$

We turn now to our calculations on dissociative and molecular adsorption of  $H_2O$  on  $SnO_2$  and  $TiO_2$  (110). The calculations are done using the same repeating-slab geometry used for the bare surface, and we need to pay attention to the effects of slab thickness and vacuum width. Another important technical question is whether it is better to perform the calculations with the particles adsorbed only on one surface of each slab or on both surfaces. We refer to these as the one-sided and two-sided geometries. There is a strong argument for working with the



Fig. 4. Atomic structure of fully hydroxylated (110) surface of rutile for a) SD, b) UD and c) SM adsorption geometries. Atom symbols as in Fig. 2, with adsorbed oxygen atoms represented by large white circles and hydrogens by small white circles.

symmetrical two-sided geometry in which the same particles are adsorbed on opposite surfaces, because any possible dipole moment of the repeated cell is then eliminated, and convergence of the adsorption energy with increasing slab thickness is likely to be improved. We have made tests which confirm that this is the case, and all our calculations have therefore been made using the two-sided geometry.

Our tests on the effects of slab thickness and vacuum width were performed on the  $\text{SnO}_2$  system in which  $\text{H}^+$  is adsorbed on top of every bridging oxygen and  $\text{OH}^-$  is adsorbed at every 5-fold Sn site (see Fig. 4a). In these tests, every atom in the system is relaxed to its equilibrium position. Using the two-sided slab geometry mentioned above, we find that increase of the vacuum width from two to three O -  $\text{Sn}_2\text{O}_2$  - O units changes the adsorption energy by only 0.01 eV per water molecule, and increase of the slab thickness from three to four units gives a change of 0.03 eV per molecule. If the one-sided slab geometry is used, the changes are nearly ten times as great. The results to be presented have all been obtained with a slab thickness of three units and a vacuum width of two units. We stress that in all the calculations that follow the entire system is fully relaxed to equilibrium.

As noted in the Introduction, we cannot be sure in advance how  $\text{H}_2\text{O}$  will prefer to adsorb. To study dissociative adsorption, we begin with the symmetrical full-coverage case mentioned above (see Fig. 4a). We then study symmetry-lowering distortions from this configuration. A similar strategy is followed for the case of molecular adsorption. The effect of going to lower coverage is than briefly examined for the dissociative case.

#### 4.1 Symmetrical dissociative adsorption (SD)

The dissociative adsorption energy is obtained from the fully relaxed total energy of the slab system in which  $\text{H}^+$  and  $\text{OH}^-$  are adsorbed at both surfaces. It is calculated in the natural way by subtracting this energy per unit cell from the corresponding energy for the bare slab plus the energy of a pair of  $\text{H}_2\text{O}$  molecules; the result is, of course, divided by two, since two  $\text{H}_2\text{O}$  molecules (one on each surface) are adsorbed per unit cell. As usual, a positive adsorption energy means that the total energy decreases when the molecule is adsorbed. In the symmetrical dissociative (SD) case, our LDA calculations for  $\text{SnO}_2$  and  $\text{TiO}_2$  (110) yield adsorption energies of 1.19 and 0.91 eV per  $\text{H}_2\text{O}$  respectively. Inclusion of gradient corrections lowers the adsorption energies considerably to 0.48 and 0.45 eV per  $\text{H}_2\text{O}$ . It is clear from this that gradient corrections have an extremely important effect on the calculated adsorption energies. A similar effect of lowering of the adsorption energy by inclusion of GGA has already been reported for adsorption on metal surfaces [44,45], leading to a substantial improvement with respect to experimental results.

We find that the dissociative adsorption of water causes the equilibrium surface structure to

Table 4

Calculated bond length modifications on hydroxylated  $\text{SnO}_2$  (110) and  $\text{TiO}_2$  (110) with respect to the bulk values for LDA (CA), and GGA (BP) forms of exchange-correlation. The modifications of O–H bond lengths are given with respect to the free  $\text{OH}^-$  molecule. For atom indexing see Fig. 4a.

	$\text{SnO}_2$		$\text{TiO}_2$	
	CA	BP	CA	BP
$\text{O}_I - \text{M}_I$	1.2%	1.5%	2.5%	2.7%
$\text{O}_{IV} - \text{M}_{II}$	2.2%	3.4%	3.8%	4.3%
$\text{O}_{II} - \text{M}_{II}$	1.1%	1.1%	1.4%	0.9%
$\text{O}_{II} - \text{M}_I$	-1.5%	-1.4%	-1.7%	-1.0%
$\text{O}_{III} - \text{M}_I$	-1.5%	-1.9%	-2.7%	-3.1%
$\text{O}_I - \text{H}_I$	-0.8%	-0.8%	-1.6%	-1.5%
$\text{O}_A - \text{H}_{II}$	-2.2%	-2.2%	-1.7%	-2.0%
$\text{O}_A - \text{M}_{II}$	-5.5%	-6.2%	-6.9%	-7.0%

change significantly. The relaxations found for the clean surface are greatly reduced and in some cases reversed. The adsorption causes 5- and 6-fold cations to move respectively out of and into the surface, the in-plane oxygens to move outward, and the bridging oxygens to move slightly outward, relative to the relaxed clean surface. Compared with free hydroxyl molecules, surface O–H bonds are considerably shorter, the shortening being especially pronounced for the OH group attached to the 5-fold surface cation. Similarly, the bond between the OH group and the surface cation is much shorter than the bulk O–cation bond, resembling rather the inter-atomic distance in the corresponding diatomic molecule. Details of inter-atomic bond length changes for both materials (with respect their perfect crystal values), with and without gradient corrections, are presented in Table 4. The changes of O–H bond lengths are given with respect to the free  $\text{OH}^-$  molecule. It is clear from the table that, in contrast to the adsorption energies, the relaxed structure of the hydroxylated surface is little affected by gradient corrections.

Figure 5a shows both total and local DOS calculated for the hydroxylated (110) surface of  $\text{SnO}_2$  and  $\text{TiO}_2$ . Two oxygen sites were studied using the LDOS: the bridging oxygen atom  $\text{O}_I$  and the oxygen of the adsorbed  $\text{OH}^-$  group  $\text{O}_A$ . Compared with clean surfaces, two main modifications are apparent:

- the contribution due to the bridging oxygen atom, situated at the top of the valence band for clean surfaces (and giving an extra feature above the O(2s) band) has been pushed towards lower energies, and hybridizes more strongly with the bulk O(2p) band. On the

Fig. 5. Calculated valence band densities of states for hydroxylated (110) surfaces of  $\text{TiO}_2$  and  $\text{SnO}_2$  in a) SD, b) UD c) SM adsorption geometries. The dashed line represents the LDOS on the bridging oxygen site  $\text{O}_I$ , and the dotted line the LDOS on the adsorbed oxygen site  $\text{O}_A$ . For the sake of presentation the local contributions have been scaled by a factor of 5.

other hand, formation of the  $\text{O-H}^+$  bond gives rise to sharp bonding  $3\sigma$  states below the  $\text{O}(2p)$  band and  $2\sigma$  states below the  $\text{O}(2s)$  band.

- the adsorbed hydroxyl group gives a contribution to the valence  $\text{O}(2p)$  band due to its occupied  $1\pi$  state. It lies above the surface VBM in the case of  $\text{SnO}_2$  (110) and within the surface VB for  $\text{TiO}_2$  (110). On the other hand, bonding  $3\sigma$  states can be seen as a narrow peak below the  $\text{O}(2p)$  band on  $\text{TiO}_2$  (110), whereas on  $\text{SnO}_2$  (110) they lie within the  $\text{O}(2p)$  band. For both materials, the  $2\sigma$  peak lies within  $\text{O}(2s)$  band. Separations of  $2\sigma - 3\sigma$  and  $3\sigma - 1\pi$  are respectively 10.3 eV and 6.2 eV for  $\text{SnO}_2$  and 11.4 eV and 5.3 eV for  $\text{TiO}_2$ .

It is clear from the results that, especially for the adsorption energy, gradient corrections make a substantial difference. All the remaining calculations are performed with the Becke-Perdew GGA scheme only.

#### 4.2 Unsymmetrical dissociative adsorption (UD)

The SD geometry described in the previous section is not the most stable one, and a small displacement of the adsorbed atoms from their fully symmetric positions makes the system relax to a configuration of lower energy. We find that this unsymmetrical dissociative (UD) configuration gives an adsorption energy of 1.39 eV per  $\text{H}_2\text{O}$  for  $\text{SnO}_2$  (110) and 1.08 eV per  $\text{H}_2\text{O}$  for  $\text{TiO}_2$  (110), so that the breaking of symmetry yields a stabilization of well over 0.5 eV.

The nature of the new relaxed configuration is shown in Fig. 4b. The bridging ( $\text{O}_I$ ) and adsorbed ( $\text{O}_A$ ) oxygens approach each other, and the proton ( $\text{H}_I$ ) attached to bridging oxygen tilts towards  $\text{O}_A$ , so as to form a hydrogen bond  $\text{O}_A\text{-H}_I$  of length 1.81 Å on  $\text{SnO}_2$  (110) and 1.80 Å on  $\text{TiO}_2$  (110). The separation between  $\text{O}_A$  and  $\text{O}_I$  oxygens is 2.78 and 2.77 Å for the two materials. These changes induce a dilation of the  $\text{O}_I\text{-H}_I$  bond (by 5.2% for  $\text{SnO}_2$  and 4.4% for  $\text{TiO}_2$ ) and smaller dilations of bonds between oxygens and surface cations.

Relaxation to the unsymmetrical configuration causes noticeable changes to the DOS and LDOS described in the previous section. We note (see Fig. 5b) a significant broadening of the isolated peak due to non-bonding  $1\pi$  states of adsorbed  $\text{OH}^-$ . In both materials, the  $3\sigma$  levels are shifted upwards and hybridize more strongly with the valence band. Similar changes can be observed in the LDOS of the  $\text{O}_I\text{-H}_I$  group, with a marked upward shift of  $3\sigma$  into the  $\text{O}(2p)$  band. The separations of the  $2\sigma - 3\sigma$  and  $3\sigma - 1\pi$  peaks become respectively 11.7 eV and 4.6 eV for  $\text{SnO}_2$  and 13.3 eV and 3.7 eV for  $\text{TiO}_2$ .

### 4.3 Symmetrical molecular adsorption (SM)

We have considered the case of symmetrical molecular (SM) adsorption in which the water molecule bonds by its oxygen to the surface 5-fold coordinated cation and the plane of the molecule is the (001) plane (Fig. 4c). We find that for both materials adsorption in this geometry is energetically favorable, the adsorption energies being 0.78 eV per H<sub>2</sub>O for SnO<sub>2</sub> and 0.82 eV per H<sub>2</sub>O for TiO<sub>2</sub>. These are considerably larger than the adsorption energies for the SD geometry. (Recall that we are comparing energies calculated with the GGA.)

We find that molecular adsorption of H<sub>2</sub>O causes only minor changes to the surface structure. Relative to the relaxed clean surface, the 5-fold coordinated cation moves out by 0.05 Å (SnO<sub>2</sub>) and 0.03 Å (TiO<sub>2</sub>). The bridging oxygen moves out somewhat less and the atoms of the first M<sub>2</sub>O<sub>2</sub> atomic plane move inwards. The size of the latter effect is nearly negligible for SnO<sub>2</sub> (110) but the displacements are as large as 0.1 Å on TiO<sub>2</sub> (110). There is also a significant deformation of the adsorbed molecule: even though the O–H bond lengths remain unchanged, the angle between the bonds is increased by 10%. This is mainly due to modification of the water 3a<sub>1</sub> orbital, because of its contribution to bonding to the surface cation. The O-cation bond between the water molecule and the surfaces is about 10% longer than the corresponding bond in the bulk crystal.

Densities of states for molecularly adsorbed water are presented in Fig. 5c. Compared with the DOS of the clean surface, the features attributed to the bridging oxygens (additional peak above O(2s) and O(2p) bands) remain practically unchanged. The modification due to adsorbed H<sub>2</sub>O can be seen as an isolated narrow peak below the O(2s) and O(2p) bands, as well as a two-peak contribution to the O(2p) band. These can be attributed to 2a<sub>1</sub>, 1b<sub>2</sub>, 3a<sub>1</sub> and 1b<sub>1</sub> molecular states respectively. The energy separations between peaks are about 11.5/2.9/3.4 eV for SnO<sub>2</sub> and 11.5/3.4/3.2 eV for TiO<sub>2</sub>, which are quite close to the free molecule results (12.0/3.6/2.1 eV), with the biggest modification, as expected, being the downward shift and a small splitting (for SnO<sub>2</sub> (110)) of the 3a<sub>1</sub> peak.

### 4.4 Surface dissociation

Of the geometries we have examined, the two most stable are the UD and the SM configurations, with the difference of adsorption energies being  $\sim 0.6$  eV for SnO<sub>2</sub> and 0.3 eV for TiO<sub>2</sub>. In both materials, dissociative adsorption is favored. It thus seems possible that water adsorbed molecularly on the surface can spontaneously dissociate. Whether or not this occurs will depend crucially on the existence and height of the energy barrier that has to be overcome when the hydrogen bond is created and when the proton migrates along it.

To investigate this problem, we have calculated the total energy of the system for a number of configurations along the probable dissociation path. In practice, we have chosen the reaction coordinate to be the horizontal (in the surface plane) separation of the 5-fold coordinated cation and the migrating proton. The positions of all other atoms, as well as the vertical position of

Fig. 6. Dependence of adsorption energy on the reaction coordinate (see text) for water dissociation on SnO<sub>2</sub> (110) and TiO<sub>2</sub> (110).

5-fold coordinated cation and of H<sub>1</sub> have been relaxed for each value of the reaction coordinate. Results on the dependence of the adsorption energy on the M<sub>1</sub>-H<sub>1</sub> horizontal separation for both materials are displayed in Fig. 6. For both materials, we find almost no energy barrier which would need to be overcome on the passage from SM to UD adsorption geometries. It is possible that there may be a very shallow minimum at the SM geometry, but this would not be of any practical significance.

#### 4.5 Adsorption in the low adsorbate density limit

In order to get insight into the dependence of adsorption characteristics on the adsorbate density we have considered the half-coverage case where there is one H<sub>2</sub>O in every two surface unit cells. Because of limitations on computer time, we have chosen a single adsorption geometry, namely the UD one, which is energetically the most favorable in the high density limit.

The practical calculations were performed with a supercell twice as big as the previous one, keeping however a slab thickness of three O - M<sub>2</sub>O<sub>2</sub> - O units and a vacuum width equivalent to two units. The clean surface calculations were repeated for this supercell in order to ensure cancellation of errors between the clean and hydroxylated slabs. The positions of all slab and adsorbate atoms were relaxed to equilibrium. We find that the adsorption energy is greater for the half-coverage case, namely 1.63 eV per H<sub>2</sub>O for SnO<sub>2</sub> (110). Compared with full coverage case, the atomic structure of the surface and adsorbate are only slightly modified.

## 5 Discussion

Our calculations on the energies of different relaxed configurations indicate that dissociative adsorption gives the largest adsorption energy and that the most stable configuration is unsymmetrical. The adsorption energies at full coverage are 1.39 and 1.08 eV per water molecule for SnO<sub>2</sub> and TiO<sub>2</sub>, increasing to 1.63 for SnO<sub>2</sub> at half coverage. It is important to note that dissociative adsorption gives the strongest binding, even though we are dealing with the perfect surface and no defects are involved. This appears to be an entirely geometrical effect, since our results are very similar for SnO<sub>2</sub> and TiO<sub>2</sub>, in spite of their different electronic structure. In fact, our entire set of results both for molecular and for dissociative adsorption, and for the instability of the molecularly adsorbed state, is remarkably similar for the two materials. Their similarity may perhaps be understood by noting that they differ mainly in their *unoccupied* electronic states.

In the TDS experiments referred to in the Introduction [10,13], the high temperature features at 435 K (SnO<sub>2</sub>) and 375 K (TiO<sub>2</sub>) were attributed to desorption from the dissociated state.

Adsorption energies can be deduced from these desorption temperatures following the analysis of Redhead [60], which expresses the desorption energy rate as the product of an effective vibrational frequency and a Boltzmann factor  $\exp(-E_{\text{ads}}/kT)$ , where  $E_{\text{ads}}$  is the adsorption energy. Assuming a frequency of  $10^{13} \text{ s}^{-1}$ , we find that this analysis gives adsorption energies of 1.1 and 1.0 eV for  $\text{SnO}_2$  and  $\text{TiO}_2$  respectively. Our calculated values are thus in fair agreement with experiment, though they are systematically too high. It is likely that this discrepancy is related to the fact that our DFT calculations – even with gradient corrections – underestimate the energy of the reaction  $\text{H}_2\text{O} \rightarrow \text{OH}^- + \text{H}^+$  (see sec. 3.2). The fact that the adsorption energy for  $\text{SnO}_2$  is greater than that for  $\text{TiO}_2$  is correctly given by our calculations.

The relation of our results to the two lower temperature peaks in the TDS spectra depends on how one interprets these peaks. The peak at the lowest temperature appears to arise from desorption of molecular  $\text{H}_2\text{O}$  when more than a monolayer is present, i.e. desorption of  $\text{H}_2\text{O}$  bound to other  $\text{H}_2\text{O}$ . Our calculations clearly have nothing to say about this. The intermediate peak at 300 K ( $\text{SnO}_2$ ) and 275 K ( $\text{TiO}_2$ ) was also attributed mainly to desorption from the molecularly bound state. Our calculations clearly suggest that molecular  $\text{H}_2\text{O}$  directly bound to the (110) surface is unstable with respect to dissociation. It is relevant to note that the semi-empirical calculations of Bredow and Jug [18] on the isolated  $\text{H}_2\text{O}$  molecule on the  $\text{TiO}_2$  (110) surface found a barrier separating the molecular and dissociated states, but the height of this barrier was only  $\sim 0.2$  eV. There are then two possible interpretations of the experiments: either the water desorbed at the intermediate temperature is not bound directly to the oxide, but is perhaps bound to hydroxyl groups; or there is some more stable molecularly adsorbed state which we have not examined. Both of these seem quite plausible. The second interpretation could be probed by making a more extensive search for stable molecularly adsorbed configurations, perhaps using dynamical simulations, and we hope to return to this.

Our calculations have predicted an appreciable increase of dissociative adsorption energy with decreasing coverage. This is consistent with experimental findings that the coverage of dissociatively adsorbed water on  $\text{SnO}_2$  and  $\text{TiO}_2$  (110) is less than a monolayer, and can be attributed to the effect of repulsion between hydroxyl groups. The same effect has been found in semi-empirical quantum calculations on the dissociative adsorption of  $\text{H}_2\text{O}$  on  $\text{TiO}_2$  [1,16].

Calculated local densities of states for the oxygen atom  $O_A$  in the adsorbed  $\text{OH}^-$  group (geometries SD and UD) or for the adsorbed water molecule (geometry SM) strongly resemble the spectra of the corresponding free molecules. The principal modification concerns the molecular orbital directly involved in formation of the bond with the surface,  $3\sigma$  for  $\text{OH}^-$  and  $3a_1$  for  $\text{H}_2\text{O}$ . In most cases modifications consist of a downward shift (relative to the free molecule) accompanied by a small splitting, and are consistent with UPS findings on hydroxylated  $\text{TiO}_2$  (110) [7]. It is also worth noticing, that for the more stable unsymmetrical geometry the peak related to nonbonding  $1\pi$  or  $1b_1$  is considerably broadened or split by the formation of a hydrogen bond and hybridization with the surface O(2p) band. On the other hand adsorption of the proton on the bridging oxygen introduces a strong modification to its LDOS. This is clearest for the symmetrical dissociative adsorption case, where the additional electrostatic field of adsorbed  $\text{H}^+$  causes a substantial downward shift of the totality of  $\text{LDOS}(O_I)$  compared to the clean surface. In addition a distinct peak due to bonding O–H states appears below O(2p) band. The

overall structure of the LDOS on bridging oxygen for dissociative adsorption is quite similar to the free molecule spectrum, although for the unsymmetrical geometry broadening and splitting of both features in the region of the O(2p) band become important.

Comparison of our results with experimental UPS spectra [7,13] shows quite good agreement. However it should be kept in mind that experimental spectra taken at low temperatures tend to show molecularly adsorbed water which may be in higher adsorbed layers, rather than being bound directly to the surface. This could explain the much closer resemblance of measured spectra to those of free molecules. On the other hand, the high-temperature spectra showing a two-peak structure which can be assigned to OH<sup>-</sup> molecular orbitals relate well to our LDOS for adsorbed oxygen. A surprising feature of the experimental results is the total absence of signal from OH groups formed on bridging oxygens, which according to our calculations should also give a characteristic, two-peak structure.

## 6 Conclusions

We have studied molecular and dissociative adsorption of water on SnO<sub>2</sub> (110) and SnO<sub>2</sub> (110) by an *ab initio*, density functional approach. We found that inclusion of gradient corrections to the LDA noticeably reduces the adsorption energies, a tendency which has been found already for surface adsorption on metals. For both materials, in the full coverage regime, we find that both molecular and dissociative adsorption are energetically favorable. However, dissociative adsorption has a substantially greater adsorption energy. Investigation of a possible reaction path for the surface dissociation of water shows the absence of any energy barrier. We found an increase of adsorption energy in the half-coverage regime, which indicates the existence of an effective repulsive interaction between adsorbed species and suggests that the most stable adsorption configurations belong to the low coverage limit. Calculated valence band DOS spectra for molecular and dissociative adsorption geometries show structures similar to these of free H<sub>2</sub>O and OH<sup>-</sup> molecules. Bonding to the surface introduces small shifts and broadening of peaks in the region of the surface valence band.

## Acknowledgement

The work of JG is supported by EPSRC grant GR/J34842. The major calculations were performed on the Intel iPSC/860 parallel computer at Daresbury Laboratory, and we are grateful for a generous allocation of time on the machine. Analysis of the results was performed using local hardware funded by EPSRC grant GR/J36266. Assistance from L. N. Kantorovich, J. M. Holender and J. A. White is also acknowledged.

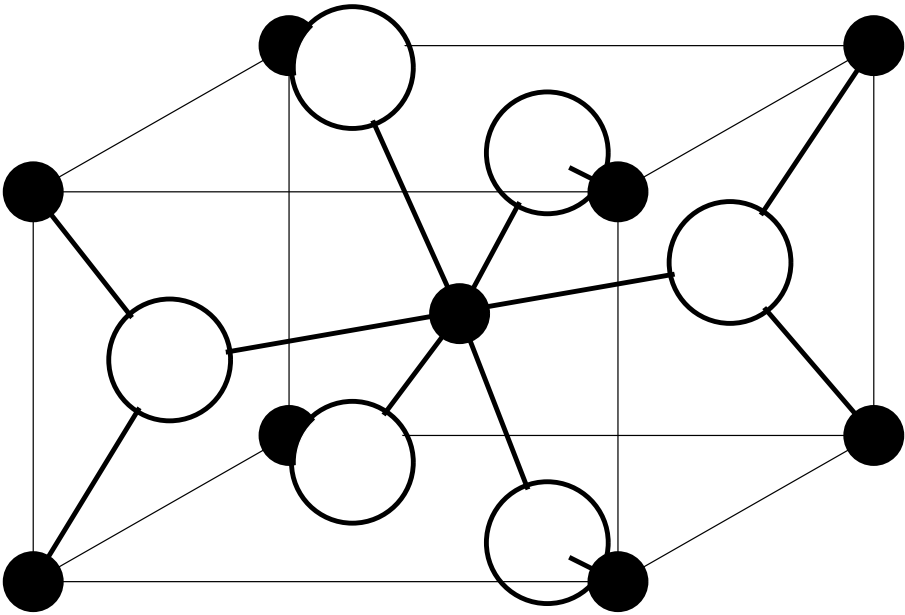
## References

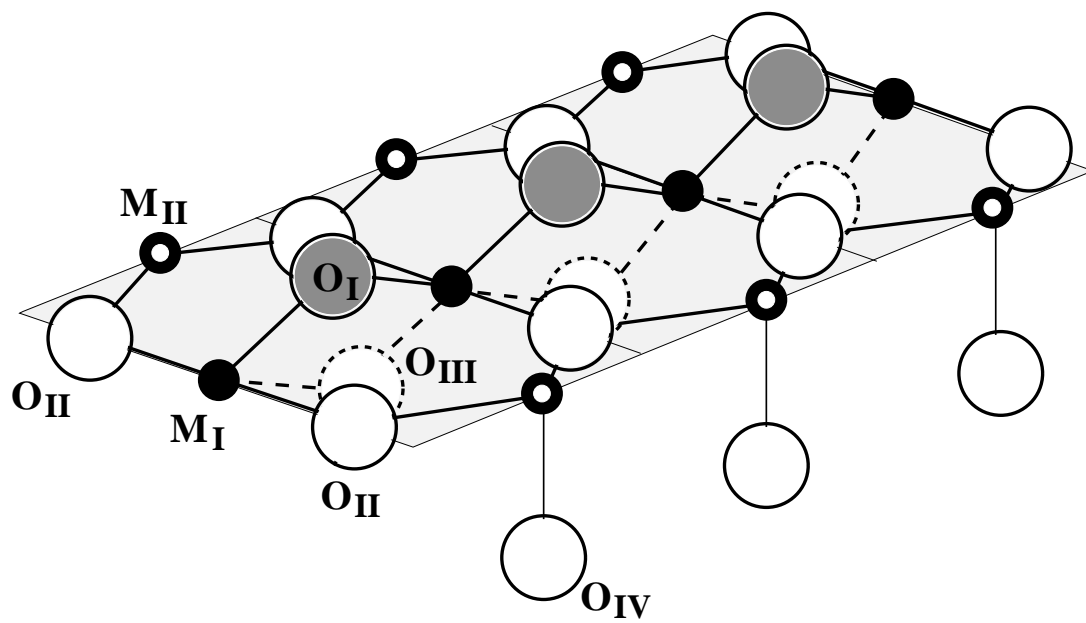
- [1] J. Goniakowski, C. Noguera, Surf. Sci. **330** (1995) 337.
- [2] W. Langel, M. Parrinello, Phys. Rev. Lett. **73** (1994) 504.
- [3] C.A. Scamehorn, N.M. Harrison, M.I. McCarthy, J. Chem. Phys. **101** (1994) 1547.
- [4] J. Tamaki, M. Nagaishi, Y. Teraoka, N. Miura, N. Yamazoe, K. Moriya, Y. Nakamura, Surf. Sci. **221** (1989) 183.
- [5] A. Fujishima, K. Honda, Nature **283** (1972) 37.
- [6] V.E. Henrich, G. Dresselhaus, H.J. Zeiger, Solid State Commun. **24** (1977) 623.
- [7] R.L. Kurtz, R. Stockbauer, T.E. Madey, E. Román, J.L. de Segovia, Surf. Sci. **218** (1989) 178.
- [8] J.-M. Pan, B.L. Maschhoff, U. Diebold, T.E. Madey, J. Vac. Sci. Technol. A **10** (1992) 2470.
- [9] C.A. Muryn, P.J. Hardman, J.J. Crouch, G.N. Raiker, G. Thornton, Surf. Sci. **251/252** (1991) 747.
- [10] M.B. Hugenschmidt, L. Gamble, C.T. Campbell, Surf. Sci. **302** (1994) 329.
- [11] G. Munera, F.S. Stone, Disc. Faraday Soc. **52** (1971) 205.
- [12] P. Jones, J.A. Hockey, Trans. Faraday Soc. **67** (1971) 2669, 2679.
- [13] V.A. Gercher, D.F. Cox, Surf. Sci. **322** (1995) 177.
- [14] M.J. Jaycock, J.C.R. Waldsax, J. Chem. Soc. Faraday Trans. I **70** (1974) 1501.
- [15] M. Tsukada, H. Adachi, C. Satoko, Prog. Surf. Sci. **14** (1983) 113.
- [16] J. Goniakowski, S. Bouette-Russo, C. Noguera, Surf. Sci. **284** (1993) 315.
- [17] A. Fahmi, C. Minot, Surf. Sci. **304** (1994) 343.
- [18] T. Bredow, K. Jug, Surf. Sci. **327** (1995) 398.
- [19] A. De Vita, M.J. Gillan, J.-S. Lin, M.C. Payne, I. Štich, L.J. Clarke, Phys. Rev. B **46** (1992) 12964.
- [20] I. Manassidis, A. De Vita, J.-S. Lin, M.J. Gillan, Europhys. Lett. **19** (1992) 605.
- [21] I. Manassidis, A. De Vita, M.J. Gillan, Surf. Sci. Lett. **285** (1993) L517.
- [22] M. Ramamoorthy, R.D. King-Smith, D. Vanderbilt, Phys. Rev. B **49** (1994) 7709.
- [23] M. Ramamoorthy, D. Vanderbilt, R.D. King-Smith, Phys. Rev. B **49** (1994) 16721.
- [24] I. Manassidis, M.J. Gillan, Phys. Rev. B, submitted.
- [25] I. Manassidis, J. Goniakowski, L.N. Kantorovich, M.J. Gillan, accepted Surf. Sci.
- [26] A.D. Becke, Phys. Rev. A **38** (1988) 3098.

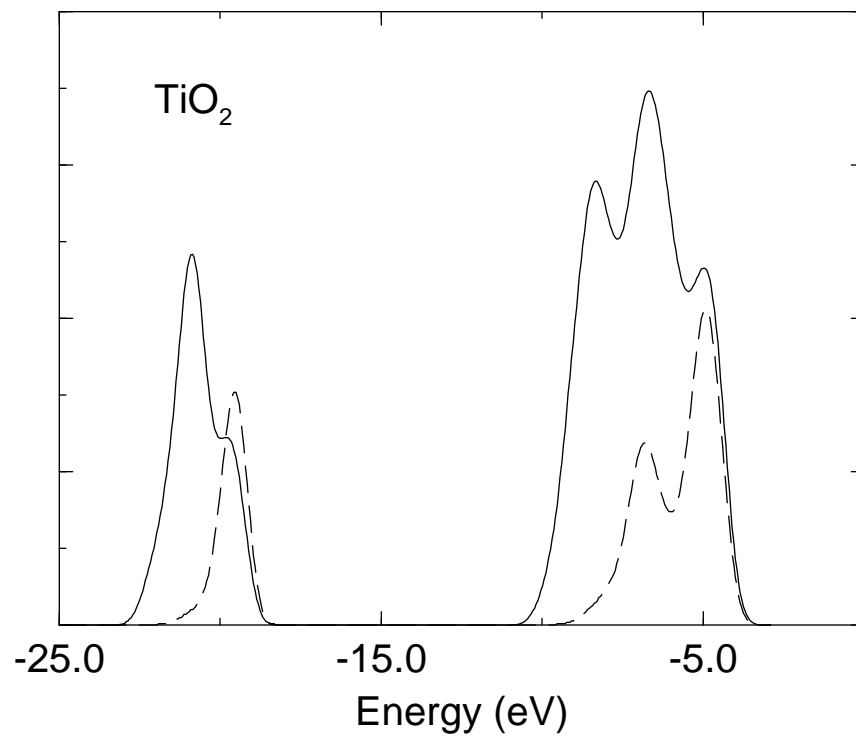
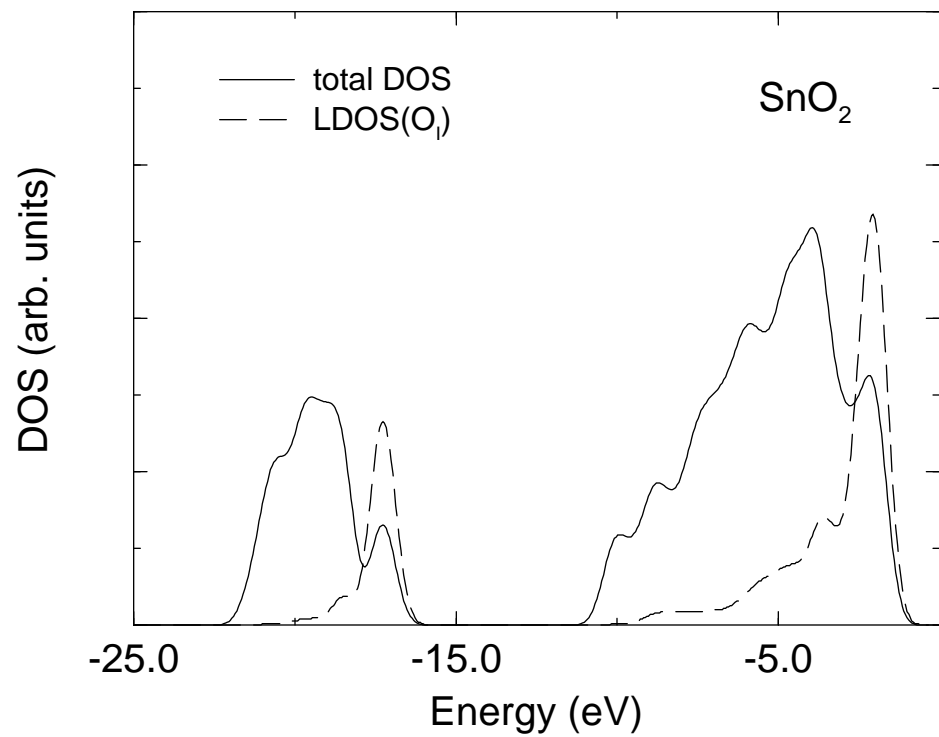


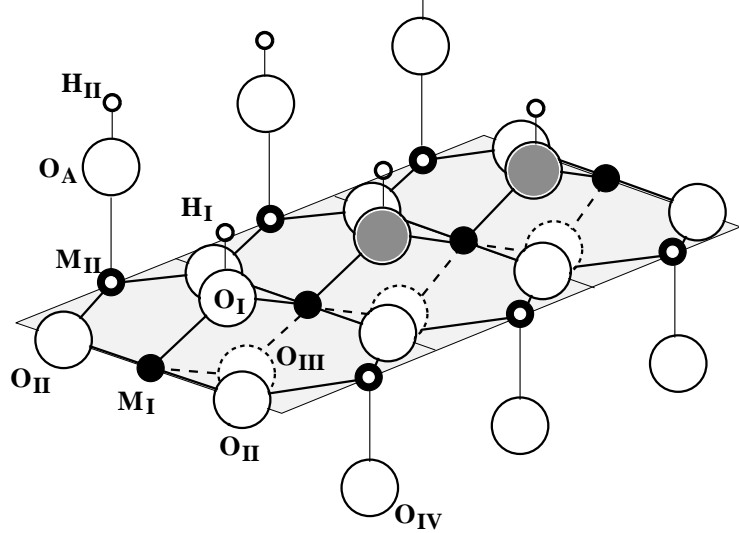
- [27] J.P. Perdew, Phys. Rev. B **33** (1986) 8822; **34** (1986) 7406(E).
- [28] P. Hohenberg, W. Kohn, Phys. Rev. **136** (1964) B864.
- [29] W. Kohn, L. J. Sham, Phys. Rev. **140** (1965) A1133.
- [30] R. O. Jones, O. Gunnarsson, Rev. Mod. Phys. **61** (1989) 689.
- [31] M. J. Gillan, in Proc. NATO ASI on Computer Simulation in Material Science, Aussois, March 1991, ed. M. Mayer and V. Pontikis, p. 257 (Dordrecht, Kluwer, 1991).
- [32] M.C. Payne, M.P. Teter, D.C. Allan, T.A. Arias, J.D. Joannopoulos, Rev. Mod. Phys. **64** (1992) 1045.
- [33] L.J. Clarke, I. Štich, M.C. Payne, Comput. Phys. Commun. **72** (1992) 14.
- [34] D.C. Langreth, M.J. Mehl, Phys. Rev. B **20** (1983) 1809.
- [35] C.D. Hu, D.C. Langreth, Phys. Scr. **32** (1985) 391.
- [36] J.P. Perdew, Y. Wang, Phys. Rev. B **33** (1986) 8800.
- [37] F.W. Kutzler, G.S. Painter, Phys. Rev. B **37** (1988) 2850.
- [38] P. Boschan, H. Gollisch, Z. Phys. D **17** (1990) 127.
- [39] P. Młynarski, D.R. Salahub, Phys. Rev. B **43** (1991) 1399.
- [40] A. García, C. Elsässer, J. Zhu, S.G. Louie, M.L. Cohen, Phys. Rev. B **46** (1992) 9829.
- [41] X.J. Kong, C.T. Chan, K.M. Ho, Y.Y. Ye, Phys. Rev. B **42** (1990) 9357.
- [42] G. Ortiz, Phys. Rev. B **45** (1992) 11328.
- [43] J.A. White, D.M. Bird, M.C. Payne, I. Štich, Phys. Rev. Lett. **73** (1994) 1404.
- [44] P. Hu, D.A. King, S. Crampin, M.H. Lee, M.C. Payne, Chem. Phys. Lett. **230** (1994) 501.
- [45] P.H.T. Philipsen, G. Tevelde, E.J. Baerends, Chem. Phys. Lett. **226** (1994) 583.
- [46] K. Gundersen, K.W. Jacobsen, J.K. Nørskov, B. Hammer, Surf. Sci. **304** (1994) 131.
- [47] J. Goniakowski, J.M. Holender, L.N. Kantorovich, M.J. Gillan, J.A. White, Phys. Rev. B, to be submitted
- [48] J.A. White, D.M. Bird, Phys. Rev. B **50** (1994) 4954.
- [49] D.M. Ceperley, B.J. Alder, Phys. Rev. Lett. **45** (1980) 566.
- [50] L. Kleinman, D.M. Bylander, Phys. Rev. Lett., **48** (1982) 1425.
- [51] J.-S. Lin, A. Qteish, M.C. Payne, V. Heine, Phys. Rev. B **47** (1993) 4174.
- [52] O. Jepsen, O.K. Andersen, Solid State Comm. **9** (1971) 1763.
- [53] G. Lehmann, M. Taut, Phys. Stat. Sol. **54** (1972) 469.
- [54] H.J. Monkhorst, J.D. Pack, Phys. Rev. B **13** (1976) 5188.

- [55] R. Wyckoff, *Crystal Structures*, 2nd. ed., vol. 1 (Interscience, New York, 1964).
- [56] M. Leslie, M.J. Gillan, *J. Phys. C: Solid State Phys.* **18** (1985) 973.
- [57] D. Eisenberg, W. Kauzmann, *The Structure and Properties of Water*, Oxford University Press, 1969.
- [58] G. Herzberg, *Spectra of Diatomic Molecules*, 2nd ed. D. Van Nostrand & Company, Inc., Princeton, N.J., 1950.
- [59] R.E. Ballard, *Photoelectron Spectroscopy and Molecular Orbital Theory*, A. Hilger Ltd., Bristol 1978.
- [60] P.A. Redhead, *Vacuum* **12** (1962) 203.

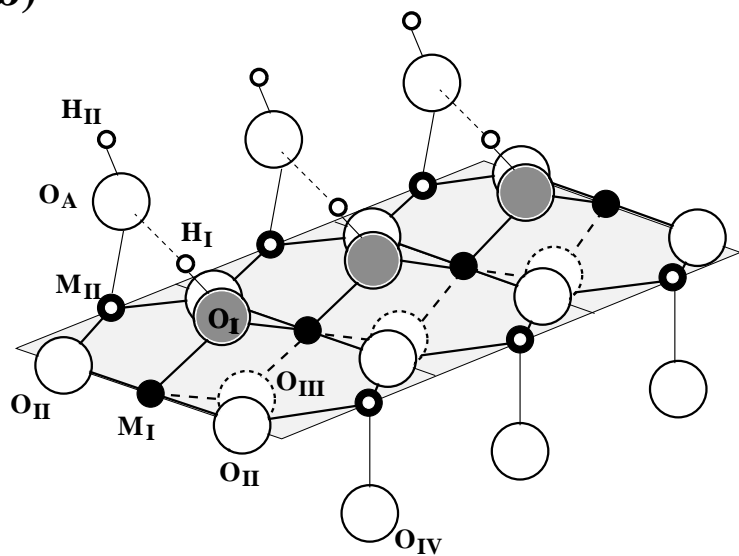




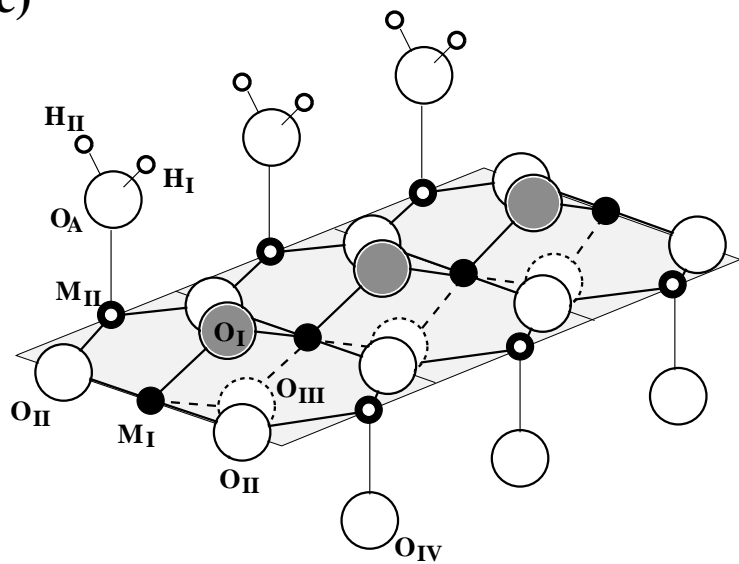




b)



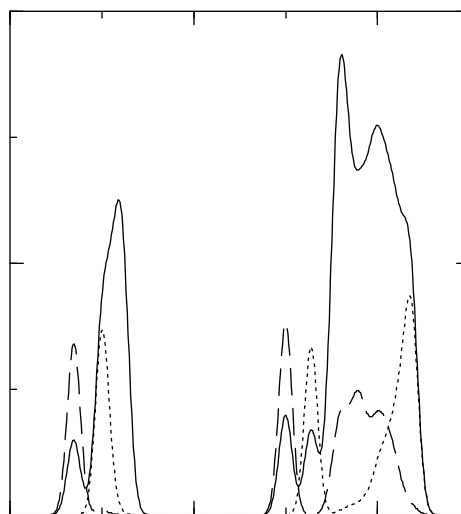
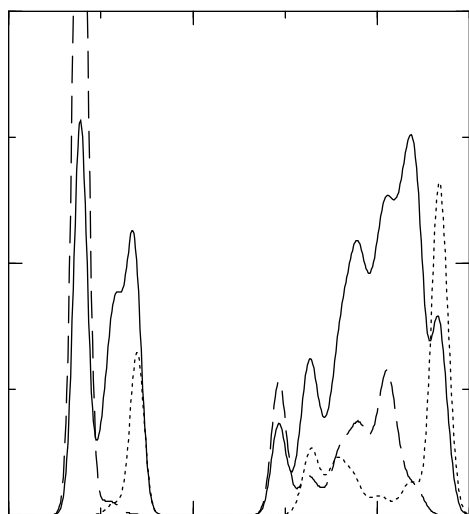
c)



SnO<sub>2</sub>

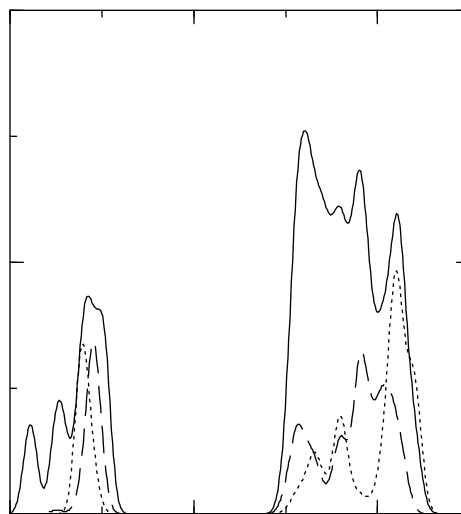
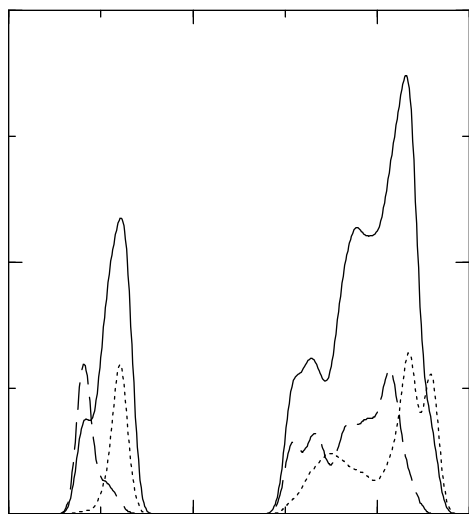
TiO<sub>2</sub>

a)

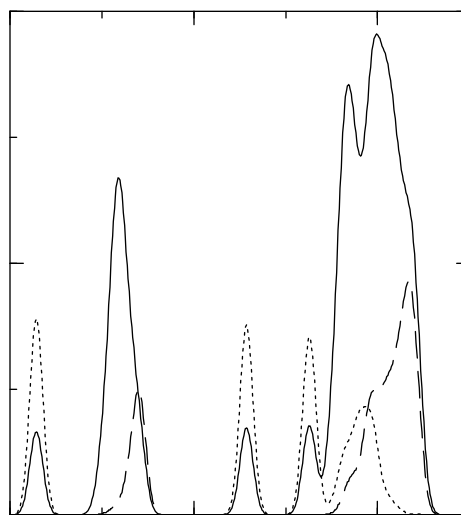
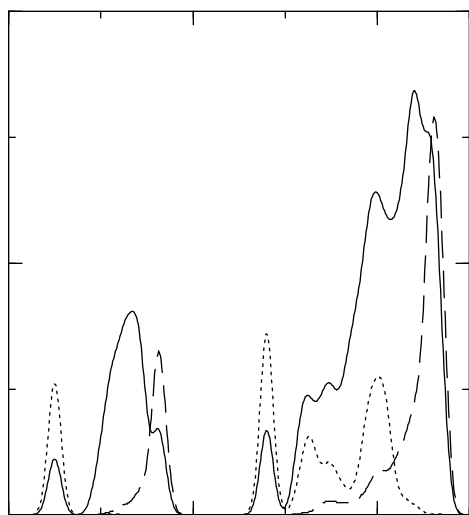


DOS (arbitrary units)

b)



c)



-25.0 -15.0 -5.0  
Energy (eV)

-25.0 -15.0 -5.0  
Energy (eV)

